

Superradiant Scattering from Nonlinear Wave-Mode Coupling

Tiemo Pedergnana* and Nicolas Noiray†

CAPS Laboratory, Department of Mechanical and Process Engineering,
ETH Zürich, Sonneggstrasse 3, 8092 Zürich, Switzerland

(Dated: March 22, 2023)

Waves scattered at a self-oscillating mode can exhibit superradiance, or net amplification of an external harmonic excitation. This exotic behavior, arising from the nonlinear coupling between the mode and the incident wave, is theoretically predicted and experimentally confirmed in this work. We propose a generic theory of nonlinear wave-mode coupling, which is derived in analogy to the temporal coupled-mode theory of [Fan et al., J. Opt. Soc. Am. A 20, 569 (2003)]. A well-reproducible aeroacoustic realization of a superradiant scatterer was used to test the theory's predictions. It is shown that the nonlinear wave-mode coupling can be exploited to quasi-passively tune the reflection and transmission coefficients of a side cavity in a waveguide. The theoretical framework used to describe this type of superradiance is applicable to non-acoustic systems and may be used to design lossless scattering devices.

Superradiance occurs when an energetic, radiating region scatters incident waves with a net amplification [1]. Paradigmatic manifestations are the Penrose process, by which particles gain momentum from a rotating black hole [2] and the Zel'dovich mechanism, where a rotating metallic cylinder increases electromagnetic oscillations [3]. Extraction of energy from rotating systems has been investigated in optics [4, 5], acoustics [6], hydrodynamics [7, 8] and quantum mechanics [9–11].

Here, we consider a scenario where superradiant scattering is achieved by using a self-oscillating cavity mode. More specifically, energy is steadily supplied to the cavity, destabilizing one of its modes to small perturbations, thus leading, under the action of internal nonlinearities, to a limit cycle $a_0 = |a_0|e^{i\omega_0 t}$ at the self-sustained angular frequency ω_0 . If an external wave with frequency $\omega \approx \omega_0$ impinges on the cavity, nonlinear wave-mode coupling (NLC) takes place, leading to an amplitude-dependent scattering matrix S exhibiting superradiance (Fig. 1). The entries of S may be tuned by varying the forcing amplitude.

To model this phenomenon, we derive a scattering theory which is related to the temporal coupled-mode theory (TCMT) of Fan et al. [12] describing unitary multipoint scattering by linearly stable resonant cavities [13–16]. In contrast, we are interested in modeling *nonlinear*, non-unitary scattering by cavities exhibiting a self-oscillating mode. Despite fruitful recent applications of coupled-mode theories in optics [17, 18], electrodynamics [19, 20], quantum mechanics [21–23] and acoustics [24–26], no analogous framework exists for nonlinear systems. This work aims to fill this gap in the literature. For simplicity, we restrict our discussion to the case of a single self-oscillating mode in a cavity with two ports.

The following set of equations is then used to model

the nonlinear scattering process:

$$\begin{aligned} \dot{a} &= (i\omega_0 + \nu - \kappa|a|^2)a + D^\dagger |s_{\text{in}}\rangle, & (1) \\ |s_{\text{out}}\rangle &= \underbrace{(C + DF^{-1}D^\dagger)}_{\text{linear}} |s_{\text{in}}\rangle + \underbrace{Da}_{\text{nonlinear}}, & (2) \end{aligned}$$

where $a \in \mathbb{C}$ is the complex modal amplitude, $(\dot{})$ is the derivative with respect to time t , $\omega_0 \in \mathbb{R}^+$ is the eigenfrequency, $\nu \in \mathbb{R}$ is the linear growth or decay rate, $\kappa \in \mathbb{R}^+$ is the nonlinearity constant, $D \in \mathbb{R}^2$ is the coupling matrix, $(\cdot)^\dagger$ is the Hermitian conjugate, $|s_{\text{in}}\rangle$ and $|s_{\text{out}}\rangle \in \mathbb{C}^2$ are the incident and outgoing waves at the forcing frequency $\omega \in \mathbb{R}^+$, $C + DF^{-1}D^\dagger \in \mathbb{C}^{2 \times 2}$ is the frequency-dependent background scattering matrix, $C \in \mathbb{R}^{2 \times 2}$ is the constant component of the background and $F \in \mathbb{C}$ is defined as $F = i(\omega - \omega_0) + \gamma$. Self-oscillation can occur only for $\nu > 0$, which is the case considered here.

The parameter $\gamma \in \mathbb{R}^+$ is the decay rate characteristic of the background process for a linearly stable resonant cavity in the absence of self-oscillation and internal nonlinearities:

$$\begin{aligned} \dot{a} &= (i\omega_0 - \gamma)a + D^\dagger |s_{\text{in}}\rangle, & (3) \\ |s_{\text{out}}\rangle &= C |s_{\text{in}}\rangle + Da. & (4) \end{aligned}$$

Equations (3) and (4) are considered here to explain the background matrix $C + DF^{-1}D^\dagger$. Together, they form the classic TCMT equations. Analogous to the constant matrix C in TCMT models, the frequency-dependent matrix $C + DF^{-1}D^\dagger$ represents the background of the nonlinear process in our theory described by Eqs. (1) and (2). This matrix, which is derived in the Supplemental Material [27], ensures linear resonant scattering for large forcing amplitudes, i.e., it bounds the nonlinear scattering process to incident waves of relatively small to moderate amplitudes [28]. A physical explanation for such a model in the specific example examined in this study is given below.

Here, we explore the theoretical framework defined by Eqs. (1) and (2) for the special case of an asymmet-

* ptiemmo@ethz.ch
† noirayn@ethz.ch

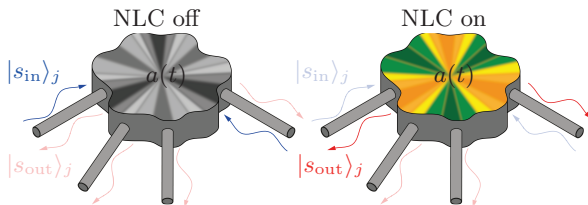


FIG. 1. In a classic resonant cavity with multiple ports (left inset), due to dissipative effects, the energy of the incident waves $\langle s_{in} | s_{in} \rangle$ always exceeds that of the outgoing waves $\langle s_{out} | s_{out} \rangle$. This limitation is overcome by inducing synchronization between the natural radiation of a self-oscillating cavity mode and the incident waves, which can lead to superradiance, or net amplification of an external harmonic excitation (right inset). The incident and outgoing waves in the j th port are denoted by $|s_{in}\rangle_j$ and $|s_{out}\rangle_j$.

ric, reflectional superradiant scatterer coupled to a one-dimensional (1D) waveguide. This choice is motivated by the nature of the present experimental realization of superradiant scattering, which is based on a classic type of aeroacoustic instability [29, 30] that has recently been revisited both theoretically and experimentally [31–33], and is accordingly well understood. Simply put, when a low-Mach air flow is incident on a cavity’s aperture at the right angle and velocity, it can destabilize one of its resonant modes, which leads to self-sustained oscillations. This transition from resonance to whistling, which can be modeled as the supercritical Hopf bifurcation associated with a Stuart–Landau oscillator [32, 34–36], is exploited in this work to create a limit cycle in the cavity, which enables superradiant scattering of harmonic waves.

In Eq. (2), the resonant nature of the background matrix $C + DF^{-1}D^\dagger$ governing scattering at large forcing amplitudes is consistent with experiments [32] and numerical simulations [37] on configurations similar to that of the experiments presented below: In [32, Fig. 8], measurements showed that the resistance of the cavity-waveguide interface in the presence of mean flow, which can take negative values when the aeroacoustic feedback is constructive, exhibits a nonlinear behavior with respect to the forcing amplitude as its value tends towards the positive constant resistance measured in the absence of flow. This saturated and *finite* positive resistance explains the resonant nature of the scattering dominated by the linear term in Eq. (2) when the forcing amplitude is sufficiently large.

In this work, the modeled linear background contains an asymmetry, the bias induced by a non-negligible mean flow inside the waveguide. Let us now discuss how we construct the associated matrices. Considering that previous works on TCMT constrained the links between γ , C and D on the basis of symmetry arguments [12, 14, 16] which are inherently difficult to generalize to non-symmetric systems, we developed another approach for deducing the coupling matrix D from two user-defined quantities: The target matrix S_* corresponding to op-

timal, resonant scattering and the matrix C , which is the frequency-independent component of the background scattering matrix. This construction of the coupling matrix can thus be used to customize the cavity-waveguide interface. In the superradiant model given by Eqs. (1) and (2), the resulting coupling matrix D also defines the contribution of the nonlinear mode a to the outgoing wave (2).

It is worth noting that the present modeling framework is by no means restricted to the example of 1D reflectional scattering considered here and may be extended to other systems in a straightforward manner by changing S_* and C , as exemplified in the Supplemental Material [27].

We follow the convention by which the diagonal and off-diagonal elements of S are reflection and transmission coefficients, respectively. To theoretically model the linear part of the scattering process, we superimpose a diagonal (reflective) target matrix S_* and a purely transmissive constant background C :

$$S_* = \begin{pmatrix} 1 + \epsilon/\sigma & 0 \\ 0 & 1 - \epsilon/\sigma \end{pmatrix}, \quad C = \begin{pmatrix} 0 & 1 \\ 1 & 0 \end{pmatrix}, \quad (5)$$

where ϵ is the asymmetry and $\sigma \in \mathbb{R}^+$ is the unitarity factor, which we introduced with the objective of accounting for internal losses, as is explained below. Formally approximating the scaled target matrix σS_* by the background matrix $C + DF^{-1}D^\dagger$ yields a low-rank approximation problem from which the unknown coupling matrix D can be determined:

$$\sigma S_* - C \approx DF^{-1}D^\dagger. \quad (6)$$

The eigenvalues μ_j and corresponding normalized eigenvectors v_j , $j = 1, 2$, of the matrix $\sigma S_* - C$ are given in the Supplemental Material [27]. To capture the main characteristics of the specified matrices σS_* and C , we define the coupling matrix D such that for resonant forcing ($F = \gamma$), the singular matrix $DF^{-1}D^\dagger$ shares with $\sigma S_* - C$ its dominant subspectrum, i.e., the eigenvalue with the largest absolute value and the corresponding eigenvector. Both D as well as the ideal parameter configuration, which we call “perfect matching”, are defined by the following two consistency conditions: (I) The spectrum of the singular matrix $D\gamma^{-1}D^\dagger$ must coincide with the dominant subspectrum of $\sigma S_* - C$. (II) For a perfectly matched scatterer with $\sigma = 1$, $C + D\gamma^{-1}D^\dagger = S_*$ must be unitary.

By the Hermiticity of the chosen S_* and C , we can expand the 2-by-2 matrix $\sigma S_* - C$ in terms of its eigenvectors $v_j \in \mathbb{C}^2$ and eigenvalues $\mu_j \in \mathbb{R}$ as follows:

$$\sigma S_* - C = \mu_1 v_1 v_1^\dagger + \mu_2 v_2 v_2^\dagger, \quad (7)$$

where $|\mu_1| \geq |\mu_2|$. To satisfy (I), we define $D = v_1 \sqrt{\gamma \mu_1}$, so that $D\gamma^{-1}D^\dagger = \mu_1 v_1 v_1^\dagger$. From (II), we deduce that

the perfect matching condition is $\epsilon = 0$. Written out, the coupling matrix D is given by

$$D = \sqrt{\gamma h(\sigma, \epsilon)} \begin{pmatrix} -g(\epsilon) \\ 1 \end{pmatrix}, \quad (8)$$

where $g(\epsilon) = \epsilon + \sqrt{\epsilon^2 + 1}$ and $h(\sigma, \epsilon) = (\sigma + \sqrt{\epsilon^2 + 1})/[\gamma(\epsilon)^2 + 1]$. As we show in the Supplemental Material [27], the asymmetry ϵ induces a biased gain in the system, which is also observed in the experiments presented below due to the presence of a mean flow with low, but non-negligible Mach number in the waveguide. Consequently, both the linear and the nonlinear part of the scattering matrix contribute to the reflectional super-radiance.

Following [16], we account for dissipative losses in the linear background process with the internal decay rate γ_i , which is related to the coupling matrix D : $D^\dagger D = 2(\gamma - \gamma_i)$ [27]. Combined with Eq. (8), this formula implies that

$$\frac{\gamma_i}{\gamma} = 1 - \frac{\sigma + \sqrt{\epsilon^2 + 1}}{2}. \quad (9)$$

The difference between γ and γ_i is the reversible decay rate $\gamma_r = \gamma - \gamma_i$. According to Eq. (9), unitary conditions ($\sigma = 1$, $\epsilon = 0$) represent a reversible background process ($\gamma = \gamma_r$). From a physical perspective, for the aeroacoustic scatterer modeled here, γ_r represents radiation losses through the ports and γ_i visco-thermal losses of the pure acoustic system in the absence of a self-oscillating mode.

The spectral low-rank approximation used above is exact when $\sigma = 1$ and $\epsilon = 0$, in which case the spectrum of $\sigma S_* - C$ is singular, and its quality decreases as $|\mu_1|$ and $|\mu_2|$ approach each other [38].

For a general model, the nonlinear scattering matrix can be obtained explicitly from the definition $|s_{\text{out}}\rangle = S|s_{\text{in}}\rangle$ and the Moore–Penrose pseudoinverse:

$$S = \frac{|s_{\text{out}}\rangle\langle s_{\text{in}}|}{\langle s_{\text{in}}|s_{\text{in}}\rangle}. \quad (10)$$

For simplicity, we focus on synchronized conditions achievable for small enough detuning and large enough forcing amplitude [27, 39]. For harmonic excitation with angular frequency ω , then, we seek the forced response \tilde{a} as the steady-amplitude solution of Eq. (1) oscillating at the same frequency. By separately applying forcing from each port with $|s_{\text{in}}\rangle = s|j\rangle e^{i\omega t}$, using Eq. (10), the NLC scattering matrix is found to be

$$S = \underbrace{C + DF^{-1}D^\dagger}_{\text{linear}} + \frac{1}{s} \underbrace{D \sum_{j=1}^2 \rho_j e^{i\varphi_j} |j\rangle}_{\text{nonlinear}}, \quad (11)$$

where $\tilde{a}_j = \rho_j e^{i(\omega t + \varphi_j)}$ is the forced response resulting from forcing the cavity through the j th port and $|j\rangle$ is the unit vector in j -direction. The frequency-dependent

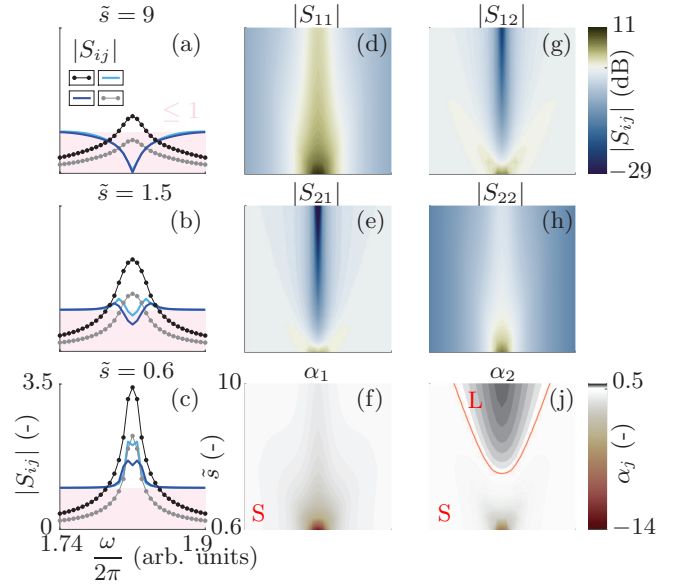


FIG. 2. Numerical example of 1D scattering for $\omega_0/2\pi = 1820$, ν equal to 0.4% of ω_0 , $\gamma = 2\nu$, $\sigma = 0.6$, $\epsilon = 0.3$ and $\kappa = 1$. Shown are (a)-(e), (g), (h) the scattering matrix coefficients $|S_{ij}|$ and (f), (j) the absorption coefficients α_j . The interval $[0, 1]$ in (a)-(c) is colored in red. The red curves in (f), (j) mark the $\alpha_j = 0$ contours, separating the domains of superradiant (S) and lossy (L) scattering. The scattering matrix S is evaluated using Eq. (14) for forcing at frequency $\omega/2\pi$ and normalized amplitude $\tilde{s} = s/\sqrt{\gamma}|a_0|$. The diagonal and off-diagonal entries of S are reflection and transmission coefficients, respectively.

quantities $\rho_j \in \mathbb{R}^+$ and $\varphi_j \in [0, 2\pi)$ satisfy Eq. (1), which is equivalent to

$$0 = \kappa^2 \rho_j^6 - 2\nu\kappa\rho_j^4 + (\nu^2 + \Delta^2)\rho_j^2 - |D_j|^2 s^2, \quad (12)$$

$$\varphi_j = -\arg D_j - \arcsin\left(\frac{\Delta\rho_j}{|D_j|s}\right), \quad (13)$$

where $\Delta = \omega - \omega_0$ is the detuning and the linearly unstable branch of φ_j has been discarded [27]. Equation (12) is a cubic equation for ρ_j^2 which, for the parameter values considered in this work, always has a single real root [27, 40]. The analytical S -matrix for a biased waveguide with two ports coupled to a nonlinear self-oscillating mode with $\nu > 0$ follows directly from Eqs. (8) and (11):

$$S = \begin{pmatrix} \frac{\gamma g(\epsilon)^2 h(\sigma, \epsilon)}{\gamma + i\Delta} & 1 - \frac{\gamma g(\epsilon) h(\sigma, \epsilon)}{\gamma + i\Delta} \\ 1 - \frac{\gamma g(\epsilon) h(\sigma, \epsilon)}{\gamma + i\Delta} & \frac{\gamma h(\sigma, \epsilon)}{\gamma + i\Delta} \end{pmatrix} + \frac{\sqrt{\gamma h(\sigma, \epsilon)}}{s} \begin{pmatrix} -\rho_1 e^{i\varphi_1} g(\epsilon) & -\rho_2 e^{i\varphi_2} g(\epsilon) \\ \rho_1 e^{i\varphi_1} & \rho_2 e^{i\varphi_2} \end{pmatrix}. \quad (14)$$

At each frequency ω , the forced response is obtained by first solving Eq. (12) for $\rho_{1,2}$ and substituting the results into Eq. (13) to compute $\varphi_{1,2}$. By prescribing different values for σ and ϵ in S_* , one can tailor D such that the nonlinear wave-mode coupling leads to superradiant scattering at a given forcing amplitude s .

We now focus on the distribution of energy of the scattered waves in the ports, which is determined by the absolute values of the entries of S , $|S_{ij}|$ [41]. We define the absorption coefficients for forcing from the j th port as $\alpha_j = 1 - |S_{1j}|^2 - |S_{2j}|^2$, $j = 1, 2$. Superradiant scattering is defined as $\alpha_j < 0$, implying a net amplification of the incident wave energy: $\langle s_{\text{out}} | s_{\text{out}} \rangle > \langle s_{\text{in}} | s_{\text{in}} \rangle$.

In the linear, symmetric and unitary limit, the energy reflection coefficient $|S_{11}|^2$ corresponds to the TCMT result of Fan et al., given by Eq. (17) of Ref. [12]. For comparison, set $\{\rho_1, \rho_2, \epsilon, \sigma\} = \{0, 0, 0, 1\}$ in Eq. (14) and $\{1/\tau, \phi, t, r\} = \{\gamma, -\pi/2, 1, 0\}$ in the reference.

A numerical example of the scattering matrix given by Eq. (14) is shown in Fig. 2 [42]. S strongly depends on the normalized forcing amplitude $\tilde{s} = s/\sqrt{\gamma}|a_0|$, undergoing a nonlinear transition from omnidirectional to purely reflectional superradiant scattering as \tilde{s} is increased. The absorption coefficients are each negative over a continuous range of amplitudes and frequencies, resulting from the energy production of the self-sustained mode. While the transition at low amplitudes is sharp, at larger amplitudes, a saturation occurs and the superradiant state persists with little change.

To confirm our theoretical analysis, a superradiant scatterer was experimentally realized by means of a self-sustained aeroacoustic mode in a side cavity which is connected to an acoustic waveguide with anechoic terminations. The cavity whistling was obtained by imposing a low Mach air flow in the waveguide with a bulk velocity that exceeds the threshold of a supercritical Hopf bifurcation. The corresponding aeroacoustic limit cycle at $\omega_0/2\pi = 1.82$ kHz involves a longitudinal mode of the cavity which constructively interacts with the coherent vorticity fluctuations in the cavity opening [29–33]. As a byproduct of the air stream, a bias on the order of the Mach number $\text{Ma} \approx 0.17$ is imposed on the system. The measured root-mean-square (rms) pressure fluctuations of the self-sustained acoustic waves radiated into the upstream and downstream sections of the waveguide are 0.54 and 0.65 hPa. The acoustic energy of the limit cycle feeds the scattered waves, enabling superradiance in the presence of incident waves.

To measure the scattering matrix S , acoustic waves produced by compression drivers placed in the anechoic ends of the waveguide are sent to the cavity. The columns S_{i1} and S_{i2} , $i = 1, 2$ are obtained separately by applying harmonic forcing upstream and downstream of the cavity. The voltage of the signal to the drivers is calibrated at each frequency to achieve a specified acoustic forcing amplitude s in the waveguide just outside the cavity aperture. Assuming lossless transmission, the multi-microphone method is employed to reconstruct the forward- and backward-propagating waves in the waveguide [43]. Details of the experimental set-up are provided in the Supplemental Material [27].

Similar to the numerical example presented in Fig. 2,

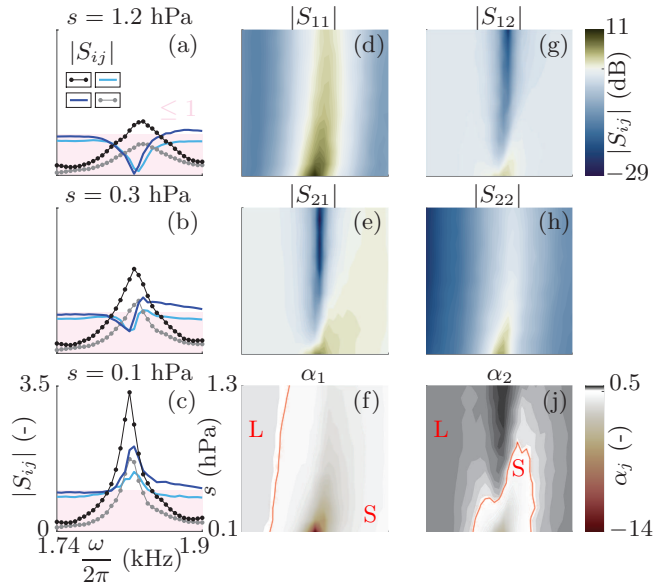


FIG. 3. Experimentally determined scattering matrix of a side cavity in a biased waveguide with two ports, when the cavity exhibits a self-oscillating aeroacoustic mode at $\omega_0/2\pi = 1.82$ kHz. Shown are the same quantities as in Fig. 2. To measure S , acoustic forcing at frequency $\omega/2\pi$ with amplitude s is applied from the two anechoic ends of the waveguide. The rms amplitudes of the acoustic waves radiated by the cavity whistling in absence of acoustic forcing are 0.54 and 0.65 hPa in the upstream and downstream sections of the waveguide.

the experimentally determined S -matrix also exhibits a nonlinear transition with increasing s from omnidirectional to purely reflectional superradiant scattering (Fig. 3). It is interesting to note that in the present biased system, superradiant reflection is stronger for incident waves in flow direction and persists at large forcing amplitudes, confirming its theoretically predicted robustness.

In the unbiased case, for $\text{Ma} = 0$ (without air flow), the scattering properties of the resonant cavity are amplitude-independent, quasi-symmetric and lossy (Fig. 4, left inset). The scattering matrix in the unbiased case is presented in detail in the Supplemental Material [27].

The self-sustained aeroacoustic system considered in this work can be compared to an electromagnetic circuit with a negative resistance element, such as a Gunn diode [44, 45] or a tunnel diode [46–48], except that the negative resistance in our case does not come from an external element but from the aeroacoustic instability which is intrinsic to the medium that the waves travel in.

We investigated both small-amplitude amplification by a Hopf bifurcation [49, 50] (see Figs. 2c and 3c) as well as scattering in the strongly nonlinear regime (see Figs. 2a and 3a). Our tunable concept is based on the synchronization between incident waves and the radiation losses of a self-oscillating source. Like in the nonlocal active metamaterial proposed in [51], destructive interferences between traveling waves in absence of the source and waves radiated from the source enable tailoring the

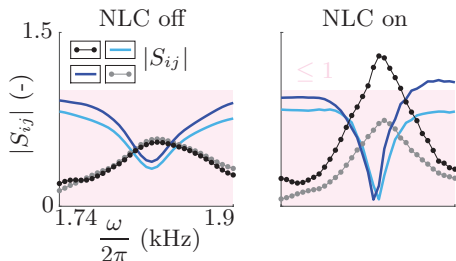


FIG. 4. Experimentally determined scattering matrix coefficients $|S_{ij}|$ at forcing amplitude $s = 1.3$ hPa for resonance-based (left inset) and limit cycle-amplified scattering (right inset). The interval $[0, 1]$ is colored in red.

scattering to quasi-perfect isolation. At the operating condition shown in Fig. 4 (right inset), the scatterer is a reflectional amplifier for waves originating from port “1” [52, 53]. We expect that the quasi-passive realization of superradiance presented in this letter will find application in flow-based acoustic metamaterials [24, 54–56], which often suffer from dissipation losses.

Future applications of our theory may also include modeling of optical scatterers such as complex nonreciprocal devices [53, 57] and spherical cavities [58]. While the derivation of the background could be performed analogously by choosing suitable matrices S_* and C , nonlinearities [59–62], negative feedback [63] or thermal noise [64] may be included through the modal equation(s). The scattering matrix follows directly from the general expression (10).

This project is funded by the Swiss National Science Foundation under Grant agreement 184617.

[1] R. Vicente, V. Cardoso, and J. Lopes, *Phys. Rev. D* **97**, 10.1103/PhysRevD.97.084032 (2018).
 [2] R. Penrose and R. Floyd, *Nat. Phys. Sci.* **229**, 177 (1971).
 [3] Y. B. Zel’dovich, *Sov. Phys. JETP* **35**, 1085 (1972).
 [4] F. Belgiorno, S. Cacciatori, M. Clerici, V. Gorini, G. Ortenzi, L. Rizzi, E. Rubino, V. Sala, and D. Faccio, *Phys. Rev. Lett.* **105**, <https://doi.org/10.1103/PhysRevLett.105.203901> (2010).
 [5] J. Drori, Y. Rosenberg, D. Bermudez, Y. Silberberg, and U. Leonhardt, *Phys. Rev. Lett.* **122**, <https://doi.org/10.1103/PhysRevLett.122.010404> (2019).
 [6] M. Crompt, G. Gibson, E. Toninelli, M. Padgett, E. Wright, and D. Faccio, *Nat. Phys.* **16**, 1069 (2020).
 [7] D. Acheson, *J. Fluid Mech.* **77**, 433 (1976).
 [8] T. Torres, S. Patrick, A. Coutant, M. Richartz, E. Tedford, and S. Weinfurter, *Nat. Phys.* **13**, 833 (2017).
 [9] J. Steinhauer, *Nat. Phys.* **10**, 864 (2014).
 [10] J. Steinhauer, *Nat. Phys.* **12**, 959 (2016).
 [11] J. Muñoz de Nova, K. Golubkov, V. Kolobov, and J. Steinhauer, *Nature* **569**, 688 (2019).
 [12] S. Fan, W. Suh, and J. Joannopoulos,

J. Opt. Soc. Am. A **20**, 569 (2003).
 [13] W. Suh, Z. Wang, and S. Fan, *IEEE J. Quantum Electron.* **40**, 1511 (2004).
 [14] Z. Wang and S. Fan, *Appl. Phys. B* **81**, 369 (2005).
 [15] V. Dmitriev, G. Portela, and L. Martins, *IEEE Trans. Microw. Theory Techn.* **66**, 1165 (2018).
 [16] Z. Zhao, C. Guo, and S. Fan, *Phys. Rev. A* **99**, <https://doi.org/10.1103/PhysRevA.99.033839> (2019).
 [17] W. Sweeney, C. Hsu, S. Rotter, and A. Stone, *Phys. Rev. Lett.* **122**, <https://doi.org/10.1103/PhysRevLett.122.093901> (2019).
 [18] H. Li, A. Mekawy, A. Krasnok, and A. Alù, *Phys. Rev. Lett.* **124**, <https://doi.org/10.1103/PhysRevLett.124.193901> (2020).
 [19] F. Alpeggiani, N. Parappurath, E. Verhagen, and L. Kuipers, *Phys. Rev. X* **7**, <https://doi.org/10.1103/PhysRevX.7.021035> (2017).
 [20] Y. Mazor, M. Cotrufo, and A. Alù, *Phys. Rev. Lett.* **127**, <https://doi.org/10.1103/PhysRevLett.127.013902> (2021).
 [21] M. Zhang, W. Sweeney, C. Hsu, L. Yang, A. Stone, and L. Jiang, *Phys. Rev. Lett.* **123**, <https://doi.org/10.1103/PhysRevLett.123.180501> (2019).
 [22] S. Franke, J. Ren, M. Richter, A. Knorr, and S. Hughes, *Phys. Rev. Lett.* **127**, <https://doi.org/10.1103/PhysRevLett.127.013602> (2021).
 [23] J. Ren, S. Franke, and S. Hughes, *Phys. Rev. X* **11**, <https://doi.org/10.1103/PhysRevX.11.041020> (2021).
 [24] R. Fleury, D. Sounas, C. Sieck, M. Haberman, and A. Alù, *Science* **343**, 516 (2014).
 [25] V. Achilleos, G. Theocharis, O. Richoux, and V. Pagneux, *Phys. Rev. B* **95**, <https://doi.org/10.1103/PhysRevB.95.144303> (2017).
 [26] C. Ferise, P. del Hougne, S. Félix, V. Pagneux, and M. Davy, *Phys. Rev. Lett.* **128**, 203904 (2022).
 [27] T. Pedergrana and N. Noiray, Supplemental Material (2022).
 [28] Note that in the steady state, due to the cubic nonlinearity in Eq. (1), the linear term dominates the nonlinear contribution to the outgoing wave (2) for large forcing amplitudes $\|C|s_{in}|\| \gg \|D\alpha_0\|$.
 [29] M. Howe, *J. Sound Vib.* **70**, 407 (1980).
 [30] S. Elder, T. Farabee, and F. DeMetz, *J. Acoust. Soc. Am.* **72**, 532 (1982).
 [31] E. Boujo, C. Bourquard, Y. Xiong, and N. Noiray, *J. Sound Vib.* **464**, <https://doi.org/10.1016/j.jsv.2019.114981> (2020).
 [32] C. Bourquard, A. Faure-Beaulieu, and N. Noiray, *J. Fluid Mech.* **909**, <https://doi.org/10.1017/jfm.2020.984> (2020).
 [33] T. Pedergrana, C. Bourquard, A. Faure-Beaulieu, and N. Noiray, *Phys. Rev. Fluids* **6**, <https://doi.org/10.1103/PhysRevFluids.6.023903> (2021).
 [34] J. Stuart, *J. Fluid Mech.* **4**, 1 (1958).
 [35] L. D. Landau and E. M. Lifshitz, *Fluid mechanics*, Vol. 11 (Pergamon Press Oxford, UK, 1959).
 [36] V. I. Arnold, *Geometrical methods in the theory of ordinary differential equations*, Vol. 250 (Springer Science & Business Media, 2012).

- [37] E. Boujo, M. Bauerheim, and N. Noiray, *J. Fluid Mech.* **853**, 386 (2018).
- [38] In the limiting case $\sigma = \epsilon = 0$, $\sigma S_* - C = -C$ has no distinguished dominant spectral subspace.
- [39] A. Balanov, N. Janson, D. Postnov, and O. Sosnovtseva, *From simple to complex* (Springer, 2009).
- [40] M. Beeler, R. W. Gosper, and R. Schroepel, *HAKMEM*, Tech. Rep. (MIT Artificial Intelligence Laboratory, 1972).
- [41] Referring to “energy” in a generic sense as the squared Euclidian norm; for a detailed discussion of acoustic energy and scattering in the presence of mean flow, see [65].
- [42] This work uses the scientific color maps of Fabio Cramerì described in Ref. [66].
- [43] S.-H. Jang and J.-G. Ih, *J. Acoust. Soc. Am.* **103**, 1520 (1998).
- [44] B. Knight and G. Peterson, *Phys. Rev.* **155**, 393 (1967).
- [45] E. Mosekilde, R. Feldberg, C. Knudsen, and M. Hindsholm, *Phys. Rev. B* **41**, 2298 (1990).
- [46] W. Bernard, H. Roth, A. Schmid, and P. Zeldes, *Phys. Rev.* **131**, 627 (1963).
- [47] H. Nguyen, D. Vishnevsky, C. Sturm, D. Tanese, D. Solnyshkov, E. Galopin, A. Lemaître, I. Sagnes, A. Amo, G. Malpuech, and J. Bloch, *Phys. Rev. Lett.* **110**, 10.1103/PhysRevLett.110.236601 (2013).
- [48] S. Fluckey, S. Tiwari, C. Hinkle, and W. Vandenberghe, *Phys. Rev. Applied* **18**, 10.1103/PhysRevApplied.18.064037 (2022).
- [49] S. Martin and W. Martienssen, *Phys. Rev. A* **34**, 4523 (1986).
- [50] E. Lacot, O. Hugon, and F. Stoeckel, *Phys. Rev. A* **67**, 10 (2003).
- [51] N. Geib, A. Sasmal, Z. Wang, Y. Zhai, B.-I. Popa, and K. Grosh, *Phys. Rev. B* **103**, 10.1103/PhysRevB.103.165427 (2021).
- [52] M. Westig and T. Klapwijk, *Phys. Rev. Applied* **9**, 10.1103/PhysRevApplied.9.064010 (2018).
- [53] Q. Zhong, S. Ozdemir, A. Eisfeld, A. Metelmann, and R. El-Ganainy, *Phys. Rev. Applied* **13**, 10.1103/PhysRevApplied.13.014070 (2020).
- [54] S. Cummer, J. Christensen, and A. Alù, *Nat. Rev. Mater.* **1**, <https://doi.org/10.1038/natrevmats.2016.1> (2016).
- [55] Y. Aurégan and V. Pagneux, *Phys. Rev. Lett.* **118**, <https://doi.org/10.1103/PhysRevLett.118.174301> (2017).
- [56] Y. Ding, Y. Peng, Y. Zhu, X. Fan, J. Yang, B. Liang, X. Zhu, X. Wan, and J. Cheng, *Phys. Rev. Lett.* **122**, <https://doi.org/10.1103/PhysRevLett.122.014302> (2019).
- [57] X.-W. Xu and Y. Li, *Phys. Rev. A* **91**, 10.1103/PhysRevA.91.053854 (2015).
- [58] H. Xie, L.-W. He, X. Shang, G.-W. Lin, and X.-M. Lin, *Phys. Rev. A* **106**, 10.1103/PhysRevA.106.053707 (2022).
- [59] M. Stephen Yeung and S. Strogatz, *Phys. Rev. E* **58**, 4421 (1998).
- [60] S. Roke, M. Bonn, and A. Petukhov, *Phys. Rev. B* **70**, 115106 (2004).
- [61] J.-B. Shim, P. Schlagheck, M. Hentschel, and J. Wiersig, *Phys. Rev. A* **94**, 10.1103/PhysRevA.94.053849 (2016).
- [62] J. Silver and P. Del’Haye, *Phys. Rev. A* **105**, 10.1103/PhysRevA.105.023517 (2022).
- [63] R. De Assis, C. Villas-Boas, and N. De Almeida, *Phys. Rev. A* **96**, 10.1103/PhysRevA.96.013821 (2017).
- [64] S. Webster, M. Oxborrow, S. Pugla, J. Millo, and P. Gill, *Phys. Rev. A* **77**, 10.1103/PhysRevA.77.033847 (2008).
- [65] Y. Aurégan and R. Starobinski, *Acta Acustica united with Acustica* **85**, 788 (1999).
- [66] F. Cramerì, G. Shephard, and P. Heron, *Nat. Commun.* **11**, <https://doi.org/10.1038/s41467-020-19160-7> (2020).